Brief Communication

MOLECULAR METABOLISM

A caveolin-1 dependent glucose-6-phosphatase trafficking contributes to hepatic glucose production

Amandine Gautier-Stein [1,*], Julien Chilloux [1], Maud Soty [1], Bernard Thorens [2], Christophe Place [3], Carine Zitoun [1], Adeline Duchampt [1], Lorine Da Costa [1], Fabienne Rajas [1], Christophe Lamaze [4], Gilles Mithieux [1,]**

ABSTRACT

Objective: Deregulation of hepatic glucose production is a key driver in the pathogenesis of diabetes, but its short-term regulation is incompletely deciphered. According to textbooks, glucose is produced in the endoplasmic reticulum by glucose-6-phosphatase (G6Pase) and then exported in the blood by the glucose transporter GLUT2. However, in the absence of GLUT2, glucose can be produced by a cholesterol-dependent vesicular pathway, which remains to be deciphered. Interestingly, a similar mechanism relying on vesicle trafficking controls short-term G6Pase activity. We thus investigated whether Caveolin-1 (Cav1), a master regulator of cholesterol trafficking, might be the mechanistic link between glucose production by G6Pase in the ER and glucose export through a vesicular pathway.

Methods: Glucose production from fasted mice lacking Cav1, GLUT2 or both proteins was measured *in vitro* in primary culture of hepatocytes and *in vivo* by pyruvate tolerance tests. The cellular localization of Cav1 and the catalytic unit of glucose-6-phosphatase (G6PC1) were studied by western blotting from purified membranes, immunofluorescence on primary hepatocytes and fixed liver sections and by *in vivo* imaging of chimeric constructs overexpressed in cell lines. G6PC1 trafficking to the plasma membrane was inhibited by a broad inhibitor of vesicular pathways or by an anchoring system retaining G6PC1 specifically to the ER membrane.

Results: Hepatocyte glucose production is reduced at the step catalyzed by G6Pase in the absence of Cav1. In the absence of both GLUT2 and Cav1, gluconeogenesis is nearly abolished, indicating that these pathways can be considered as the two major pathways of *de novo* glucose production. Mechanistically, Cav1 colocalizes but does not interact with G6PC1 and controls its localization in the Golgi complex and at the plasma membrane. The localization of G6PC1 at the plasma membrane is correlated to glucose production. Accordingly, retaining G6PC1 in the ER reduces glucose production by hepatic cells.

Conclusions: Our data evidence a pathway of glucose production that relies on Cav1-dependent trafficking of G6PC1 to the plasma membrane. This reveals a new cellular regulation of G6Pase activity that contributes to hepatic glucose production and glucose homeostasis.

Keywords Liver; Glucose-6 phosphatase; Gluconeogenesis; Intracellular glucose transport; Caveolin 1

1. INTRODUCTION

The development of type 2 diabetes is associated with the overactivation of hepatic glucose production (HGP) [1]. Indeed, although the kidney and intestine may also contribute to endogenous glucose production (EGP), HGP is preponderant during the fed post-absorptive states [2]. Moreover, we demonstrated that the lack of HGP protects against the development of insulin resistance and obesity induced by a high-fat high-sucrose diet [3]. Deciphering the regulatory mechanisms of HGP is thus needed to help prevent the worldwide burden of type 2 diabetes.

Glucose-6 phosphatase (G6Pase), the mandatory enzyme of EGP, which catalyzes the production of glucose from glucose-6 phosphate (G6P), plays a causal role in the deregulation of HGP [4]. This enzyme - composed of two functionally-linked proteins, the G6P transport subunit (G6PT) and catalytic subunit (G6PC1) - catalyzes the production of glucose from glucose-6 phosphate (G6P) [5]. Glucose production in the blood is considered as a 2-step process: the first step comprises glucose synthesis in the endoplasmic reticulum (ER) by G6Pase and the second step consists of transport across the plasma membrane by the facilitating transporter GLUT2 [6]. The localization of G6Pase mainly in the ER was demonstrated in the fifties by enzymatic assays after

[1]Université Claude Bernard Lyon 1, Université de Lyon, INSERM UMR-S1213, F-69374, Lyon, France [2]Center for Integrative Genomics, University of Lausanne, Genopode Building, 1015, Lausanne, Switzerland [3]Laboratoire de Physique (UMR CNRS 5672), ENS de Lyon, Université de Lyon, F-69364, Lyon cedex 07, France [4]Institut Curie, PSL Research University, INSERM U1143, CNRS UMR 3666, Membrane Mechanics and Dynamics of Intracellular Signaling Laboratory, 75005, Paris, France

*Corresponding author. E-mail: amandine.gautier-stein@univ-lyon1.fr (A. Gautier-Stein).

**Corresponding author.

Received December 8, 2022 • Revision received February 15, 2023 • Accepted February 24, 2023 • Available online 2 March 2023

cellular fractionation [7,8] and then confirmed by enzyme histochemistry and electron microscopy [9]. Additional biochemical studies concluded that, contrary to the other enzymes of the gluconeogenesis/glycolysis pathways, both subunits of the G6Pase complex (G6PC1 and G6PT) are deeply embedded in the ER membrane [5]. Of, note, this ER-localization is independent of the KK conserved motif identified in both G6PC1 and G6PT [10,11]. Using fluorescent chimera proteins, we recently confirmed the preponderance of the localization in the ER of both G6PT and G6PC1(12). However, the purpose of this specific location, often discussed in the past, has remained elusive [13].

A widespread dogma is that, in the short-term, glucose production and transport are controlled by the concentrations of their respective substrates G6P and glucose [5]. However, we provided numerous pieces of evidence showing that hormonal and nutrient signals control G6Pase activity and HGP on the short term [14–18]. Particularly, the acute stimulation of G6Pase activity by glucagon results in an increased glucose production by hepatocytes [19]. This activation is blunted at 21 °C, suggesting that membrane fluidity and/or mechanisms involving vesicle trafficking may control glucose production by G6Pase [20]. Interestingly, glucagon also mobilizes a vesicular pathway of glucose export, parallel to GLUT2, but dependent on cholesterol trafficking, which remains to be deciphered [21,22]. Intracellular cholesterol distribution can be regulated by Caveolin-1 (Cav1). Caveolin-1 is a 22 kDa fatty acid- and cholesterol-binding protein required for the formation of caveolae, but it is also involved in signaling pathways and energy metabolism [23,24]. Caveolin-1 proteins are embedded in the ER membrane and oligomerize immediately after synthesis in the ER [25]. Then, they associate with cholesterol in the Golgi complex in higher molecular weight complexes, which are finally transported *en route* to the plasma membrane as a disk. Cavin-1 is then recruited to these Cav1 complexes to form caveolae by invaginating the plasma membrane [25,26]. Outside caveolae, Cav1 proteins are organized as oligomers or scaffolds, which are dynamic assemblies that control membrane lipid composition, organize and transport lipids such as cholesterol and interact with several proteins [24]. Caveolin-1 proteins are mainly expressed in the adipose tissue but are also detected in the liver. Hepatic Cav1 has an important role in lipid metabolism, in particular during adaptation to fasting [27,28]. In the liver, non-caveolar Cav1 proteins are present in the ER and Golgi complex [29]. Thus, we hypothesized that Cav1 might be the mechanistic link between glucose production by G6Pase in the ER and glucose export through a vesicular pathway.

2. MATERIAL AND METHODS

2.1. Animal models

We used male adult B6. Cav1$^{-/-}$, B6.L.Glut2$^{-/-}$ [30], B6.L.G6pc$^{-/-}$ [31], B6.L.Glut2$^{-/-}$.Cav1$^{-/-}$ and wild-type (WT) mice. Liver-specific deletions of *Glut2* and *G6pc1* were obtained by tamoxifen injection at 8 weeks of age [30] and were confirmed at the mRNA levels (Supplemental Figs. 1A and B). All mice were housed in groups in the animal facility of Lyon 1 University (*Animaleries Lyon Est Conventionnelle and Specific Pathogen Free*) in controlled temperature (22 °C) conditions, with a 12-hour light-12-hour dark cycle with free access to water and standard rodent chow diet. Procedures were performed in accordance with the principles and guidelines established by the EU Directive 2010/63/EU for animal experiments.

2.2. Cell culture and plasmids

Primary hepatocytes were obtained from male mice after 16 h fasting by collagenase perfusion of the liver [32]. HepG2 cells were cultured as described previously [12]. The pcDNA3-G6PC1 and G6PC1-mCherry plasmid constructs were generated by introducing human *G6PC1* cDNA into pcDNA3 and pmCherry-N1 vectors as described previously [12]. The Ad-G6PC1-SBP-GFP construct was obtained by replacing the VSVG cDNA in the Str-Ii_VSVG-SBP-EGFP plasmid (addgene #65300) [33] by the human *G6PC1* cDNA sequence and placed in an AAV5-backbone (Laboratoire de Therapie Genique, U649, Nantes). Cav1-GFP was a gift from Ari Helenius [34].

2.3. Determination of hepatocyte glucose production

Hepatocytes were seeded into 6-well plates at 500,000 cells/well and cultured for 1 h at 37 °C in a 5% CO2 air atmosphere in DMEM without glucose supplemented either with 10 mM lactate and 1 mM pyruvate or with 1 mM pyruvate and 0.5 μCi of [2−^{14}C] pyruvate when indicated in the figure legends. After centrifugation (5min, 280 g), glucose was measured in the supernatant (extracellular glucose) and cell pellet (intracellular glucose) by enzymatic assay [35] (referred as *total glucose* in the figure legends) or [^{14}C] measurement (referred as *glucose from pyruvate* in the figure legends). [^{14}C] Glucose amount was determined from [^{14}C]-radioactivity after separation of glucose from charged metabolites by passage of supernatants or cell lysates on anion- and cation-exchangers (Dowex AG1-X8 and 50 W-X8, respectively, from Bio-Rad) as described previously [36]. The amount of glucose was normalized to the number of cells and expressed in nmol/millions of cells.

Adenovirus treatment of HepG2 cells was performed 24hrs after seeding by treating 300,000 cells per well overnight with 50pi/cell of G6PC1-SBP-GFP adenovirus (GFP adenovirus was used as control). The medium was then replaced with complete medium and cells were further incubated for 24hrs prior to the determination of glucose production. To this end, cells were placed for 1 h in DMEM without glucose supplemented with 1 mM pyruvate. Glucose was then measured in the supernatant by enzymatic assay [35]. Cells were then placed in complete DMEM medium with 80 μM biotin for 2 h. After biotin treatment, culture medium was removed and cells were further placed for 1 h in DMEM without glucose supplemented with 1 mM pyruvate. Glucose was then measured in the supernatant by enzymatic assay [35]. Glucose production was compared before and after biotin treatment for each well.

2.4. Tissue sampling, biochemical assays, protein and mRNA analyses

Mice were killed by cervical dislocation after 16 h fasting or after 6 h of refeeding (preceded by an overnight fast). The liver was quickly frozen within tongs cooled in liquid nitrogen N2 after the death of the mouse and conserved at −80 °C until analysis. Liver lysate was prepared at 4 °C and immediately processed. Hepatic G6Pase activity was assayed at maximal velocity (20 mmol/l of G6P) at 30 °C by complexometry of inorganic phosphate (Pi) produced from G6P. The phosphohydrolyzing activity toward β-glycerophosphate (20 mmol/l) was determined and subtracted from the total G6Pase activity in all cases to clear the specific G6Pase activity from the contribution of nonspecific phosphatases [37]. Glucose 6-phosphate and glycogen concentration was determined from liver lysate after deproteinization with perchloric acid (6% V/V) and neutralization with K_2CO_3 [38]. The NADPH produced from the hydrolysis of G6P by G6PDH was then used to calculate G6P content [38]. After neutralization of the lysate, glycogen was digested into glucose with α-amyloglucosidase, then glucose was measured as described [35]. Total hepatic lipids were extracted by the method of Bligh and Dyer [39] and triglyceride content was measured using a Biomerieux colorimetric kit.

For immunoprecipitation studies, protein lysates were extracted from 50 mg of WT and Cav1$^{-/-}$ liver using a Dounce homogenizer as described in [40] and used for Cav1 immunoprecipitation using rabbit anti-Cav1 antibodies (#3238, Cell Signaling). About 10% of the lysate was used for Cav1 immunoprecipitation. Immunoprecipitated proteins were then revealed by western-blotting using the rabbit anti-G6PC1 [41] and the secondary mouse Anti-rabbit IgG (Conformation Specific) (L27A9) mAb to avoid the detection of rabbit Igg chains (#5127, Cell Signaling). Purification of plasma and ER membranes was performed as described in [40] from 500 mg of WT and Cav1$^{-/-}$ liver. This protocol allowed to separate crude plasma membrane (PM) from microsomes (containing both ER and Golgi complex membranes) thanks to differential centrifugation. Western blots were performed from 5 µl of each fraction using antibodies against G6PC1 [41], E-Cadherin (#3195, Cell Signaling), Cav1 (#3238, Cell Signaling), G6PT (#NBP2-31972, Novus Biologicals) and PERK (#5683, Cell Signaling) as described previously [42]. Antibody specificity was confirmed using WT, Cav1$^{-/-}$ and L.G6pc$^{-/-}$ tissues (Supplemental Figs. 2A–D). The relative amount of total proteins was used for normalization. The contamination of plasma membrane fractions with ER membranes was assessed by the quantification of the ER resident PERK in the PM and ER fractions (Supplemental Figs. 2E and F). Chemiluminescent signals were acquired with the Chemidoc Imaging System (Biorad) and quantified using Image Lab software.

Total RNAs were extracted from frozen tissues using Trizol reagent, according to the manufacturer's instructions. mRNA levels were determined by RT-qPCR. Ribosomal protein L19 (RPL19) was used as a housekeeping gene. Calculations were based on the comparative cycle threshold method ($2^{-\Delta\Delta Ct}$).

2.5. Imaging studies

HepG2 cells were grown on high precision cover glasses and transfected using JetPrime with 125 ng of plasmid constructs per 10,000 cells. Images were acquired in living cells 48 h after transfection at 37 °C in a 5% CO_2 air atmosphere with a 63× oil-immersion objective to obtain maximal signal without any saturated pixels, either with a confocal microscope (Zeiss 880) or a DMI4000 microscope (Leica Microsystems) equipped with a spinning disk unit for 10–20 s every 0.15 s to follow protein trajectories. For total internal reflection fluorescence microscopy (TIRFM) studies, images were acquired using an EMCCD camera (Hamamatsu C9100, pixel size: 16 µm) mounted on a TIRF microscope (Leica DMI6000) equipped with a 100× oil-immersion objective (HCX PL FLUOTAR, Leica/numerical aperture = 1.46), every 0.15s (TIRF penetration 90 nm/laser line 635 nm/Quad filter 405-488-561-635 nm). Images were analyzed using Icy software to define and count spots (Spot detector [43] and Spot tracking [44] plugins) and to analyze trajectories (Motion profiler and Tracking performance measures [44] plugins). For the latter, parameters were set using random images to avoid unspecific pairing between trajectories. Based on their net travelled distance, we discriminated proteins exhibiting a directed motion from proteins moving around the same position over time.

Primary hepatocytes (24 h after seeding) and tissues were fixed with 4% paraformaldehyde. Immunofluorescence assays were performed using G6PC1, Cav1, Calnexin (#ab22595, Abcam), and Giantin (#ab37266, Abcam) antibodies with sequential tyramide signal amplification, using 640 R-tyramide for G6PC1, 488 A-tyramide for Cav1 and 568-tyramide for Calnexin/Giantin. Images were acquired with a confocal microscope (Zeiss 880) using an 63× oil-immersion objective. Image analyses were performed using FiJi and colocalization (M1 Manders and Pearson correlation coefficients) was quantified by the JaCoP plugin [45] after background subtraction.

For the transmission electron microscopy (TEM) studies, the liver zone was cut into small pieces (<1 mm) which were fixed for 2hr at 4 °C in a buffer composed of 10 mM metaperiodate, 75 mM lysine and 2% paraformaldehyde in 37 mM Sorensen's phosphate buffer complemented with 0.2% glutaraldehyde. After washes and dehydratation, pieces of tissues were embedded in pure LRWhite for polymerization at 50 °C for 48 h. Ultrathin sections (approximately 70 nm thick) were cut on a Reichert ultracut E (Leica) ultramicrotome, mounted on 200 mesh nickel polylysine coated grids. Immunogold labeling was performed by flotation on drops using rabbit G6PC1 and mouse Cav1 primary antibodies and gold conjugated secondary antibody. Sections were observed with a transmission electron microscope JEOL 1400JEM (Tokyo, Japan) operating at 80 kV equipped with a camera Orius 1000 gatan and Digital Micrograph.

2.6. Pyruvate and glutamine tolerance tests

Pyruvate tolerance tests were performed in mice fasted for 16 h. Glutamine tolerance tests were performed in mice fasted for 6 h [46]. Mice were injected intraperitoneally either with L-pyruvate or with L-glutamine (2 g/kg body weight). Blood glucose levels were determined from the tail vein at 0, 15, 30, 45, 60 and 90 min after injection, using a glucometer.

2.7. Statistical analyses

All data are presented as mean ± SEM. Two-group comparisons were analyzed using unpaired t tests. Groups were compared using one-way or two-way ANOVA followed by Tukey's post hoc tests. Analyses were performed using Prism8 software. Statistical details and exact value of n can be found in the figure legends.

2.8. Data and resource availability

Further information and requests for resources and reagents should be directed to and will be fulfilled by Amandine Gautier-Stein (amandine.gautier-stein@univ-lyon1.fr).

3. RESULTS

3.1. Glucose production by hepatocytes is inhibited in the absence of Caveolin-1

In line with our hypothesis, Cav1$^{-/-}$ primary hepatocytes produced in the culture medium about 50% less glucose from ^{14}C-pyruvate than WT hepatocytes (Figure 1A). This decrease was not compensated by a proportional increase in intracellular glucose levels, suggesting that the absence of Cav1 did not induce a decrease in glucose export but rather resulted in inhibition of glucose synthesis (Figure 1A, hatched bars). To confirm these results obtained *in vitro*, we assessed HGP *in vivo* by a pyruvate tolerance test. The increase in blood glucose levels following intraperitoneal pyruvate injection was lower in Cav1$^{-/-}$ compared to WT mice (Fig. 1C). In the Cav1$^{-/-}$ liver, intracellular G6P and glucose levels were slightly increased compared to WT levels (Fig. 1B), suggesting that, *in vivo*, the absence of Cav1 reduced glucose synthesis and glucose transport.

As Cav1 is known to be needed for the proper stabilization and signaling of the insulin receptor (IR) in adipocytes [47], we studied insulin signaling in the liver of Cav1$^{-/-}$ mice. Western-blot analyses showed that the phosphorylation levels of AKT (the main downstream target of IR signaling) were increased in the liver of refed Cav1$^{-/-}$ mice, compared to AKT phosphorylation levels in the WT liver

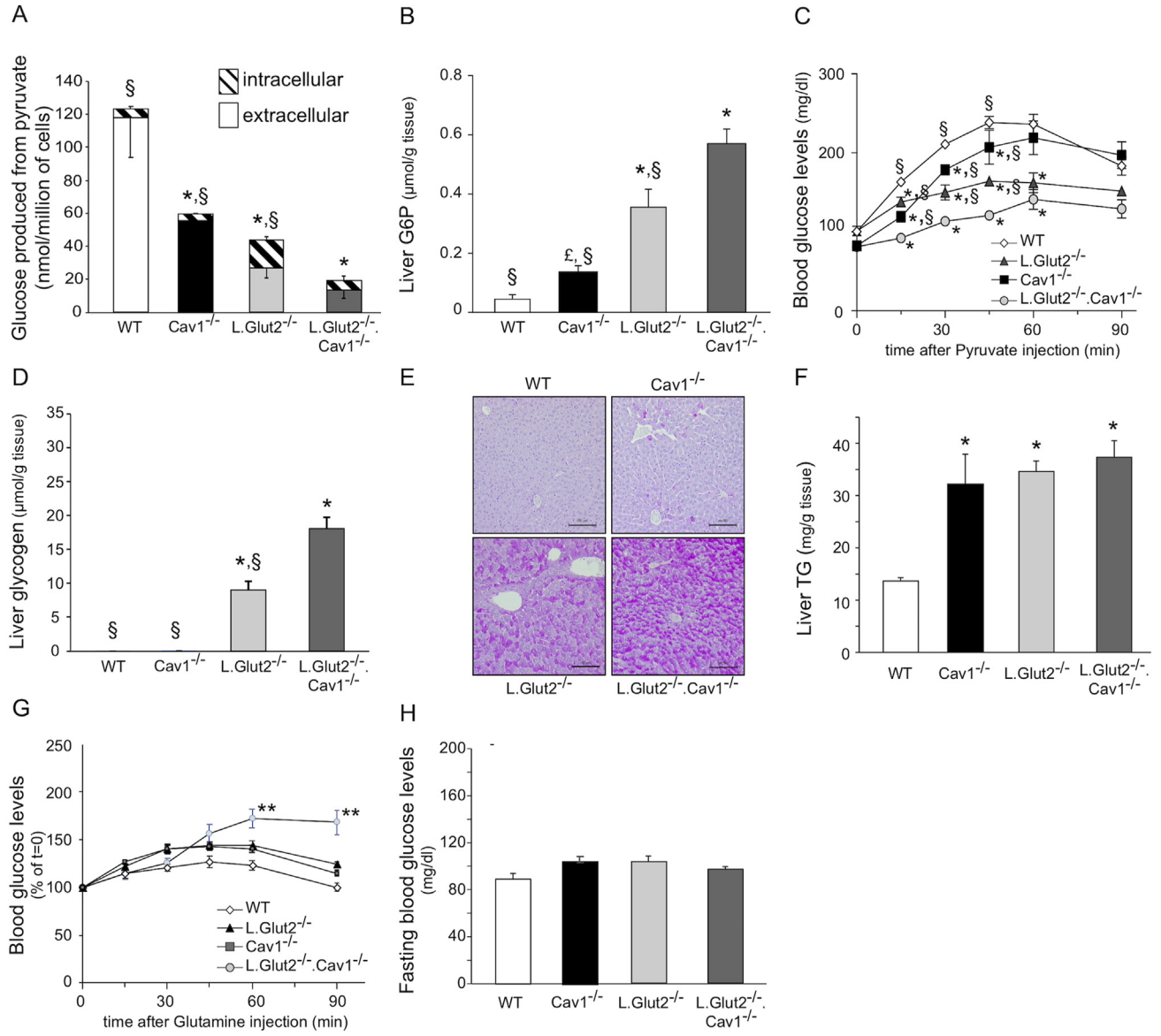

Figure 1: ***Glucose production by hepatocytes is inhibited in the absence of Caveolin-1.*** (A) Glucose produced from [^{14}C]-pyruvate by WT (white bar), Cav1$^{-/-}$ (black bar), L. Glut2$^{-/-}$ (light grey bar) and L. Glut2$^{-/-}$.Cav1$^{-/-}$ (dark grey bar) hepatocytes. Plain bars represent extracellular glucose while hatched bars represent intracellular glucose. (B) Glucose-6-phosphate (G6P) level content in mouse liver. (C) Pyruvate tolerance test after 16 h fasting. Blood glucose levels were measured every 15 min for 90 min. Glycogen (D) and triglyceride (TG) (F) content in mouse liver. Significant differences from WT are indicated as * $p < 0.01$, from L. Glut2$^{-/-}$.Cav1$^{-/-}$ as §$p < 0.01$, two-way ANOVA followed by Tukey's post hoc test. £ $p < 0.05$, for comparison between WT and Cav1$^{-/-}$ using multiparametric *t* test. Data are means ± s. e.m. from 7 to 11 mice per group. (E) Representative PAS-stained liver section. (G) Glutamine tolerance test after 6 h fasting. Blood glucose levels were measured every 15 min for 90 min. Significant differences from values before glutamine injection are indicated as **$p < 0.01$, one-way ANOVA followed by Tukey's post hoc test. (H) Blood glucose levels measured after 16 h fasting. Data are means ± s. e.m. from 15 mice per group.

(Supplemental Fig. 3). This result might suggest that a higher liver insulin sensitivity could be responsible for the decreased HGP in fasted Cav1$^{-/-}$ mice. However, gluconeogenic gene expression was not decreased in the liver of Cav1$^{-/-}$ mice fasted for 16 h compared to WT mice (Supplemental Fig 1.C-E). Accordingly, G6Pase activity, measured at Vmax in the presence of 20 mM of G6P, was similar in Cav1$^{-/-}$ and WT liver (Supplemental Fig. 4A), showing that the decrease in glucose production from Cav1$^{-/-}$ hepatocytes was not linked to a decrease in total G6Pase dephosphorylation capacity. Taken together, our results suggest that gluconeogenesis depends on a Cav1-dependent pathway in addition to the known GLUT2 pathway.

3.2. Gluconeogenesis is nearly abolished in the absence of both Caveolin-1 and GLUT2

As Cav1 is known to control glucose transport by GLUT4 in adipocytes [47], we studied whether GLUT2 might be responsible for the decreased HGP of Cav1$^{-/-}$ mice, by crossbreeding Cav1$^{-/-}$ mice with L. Glut2$^{-/-}$ mice. Glucose production from ^{14}C-pyruvate (gluconeogenesis) in L-Glut2$^{-/-}$.Cav1$^{-/-}$ hepatocytes was almost totally suppressed, compared to hepatocytes of WT, L. Glut2$^{-/-}$ or Cav1$^{-/-}$ mice (Fig. 1A), independently of a decrease in total G6Pase activity (Supplemental Fig. 4A), demonstrating that both GLUT2 and Cav1 participated independently to the control of HGP. Moreover, the total

production of glucose (glycogenolysis and gluconeogenesis) was decreased by more than 50% in L-Glut2$^{-/-}$.Cav1$^{-/-}$ hepatocytes fasted for 16 h (Supplemental Fig. 4C). In fasted L-Glut2$^{-/-}$ hepatocytes, the total production of glucose was the same as in WT, as previously described [21,22] and did not depend on the presence of pyruvate in the culture medium (Supplemental Fig. 4C), suggesting that fasted L. Glut2$^{-/-}$ hepatocytes produced glucose mainly *via* glycogenolysis rather than gluconeogenesis. Accordingly, gluconeogenesis from ^{14}C-pyruvate was 4-fold lower in L. Glut2$^{-/-}$ than in WT hepatocytes (Fig. 1A), independently of a decrease in total G6Pase activity (Supplemental Fig. 4A). The lower gluconeogenesis in L-Glut2$^{-/-}$ and L-Glut2$^{-/-}$.Cav1$^{-/-}$ mice was also confirmed *in vivo* by a PTT (Fig. 1C). In addition, L-Glut2$^{-/-}$ and L-Glut2$^{-/-}$.Cav1$^{-/-}$ livers accumulated high levels of G6P (Fig. 1B), glycogen (Figure 1D,E) and TG (Fig. 1F). Interestingly, the increases in hepatic G6P and glycogen were doubled in L-Glut2$^{-/-}$.Cav1$^{-/-}$ compared to L-Glut2$^{-/-}$ mice, suggesting a stronger suppression in G6P hydrolysis in L-Glut2$^{-/-}$.Cav1$^{-/-}$ livers (Figure 1B,D). Consistent with an increase in hepatic TG content, the expressions of *Lpk* and *Fasn* (coding for the main regulatory glycolytic and lipogenic enzymes, respectively) were considerably increased in the livers of L-Glut2$^{-/-}$ and L-Glut2$^{-/-}$.Cav1$^{-/-}$ mice (Supplemental Figs. 1F and G). Of note, only L. Glut2$^{-/-}$.Cav1$^{-/-}$ liver exhibited increased expression of *Scd1*, coding for the stearoyl-CoA desaturase 1 (Supplemental Fig. 1H), in accordance with the induction of *de novo* lipogenesis by accumulated G6P, as previously described [3]. To resume, L. Glut2$^{-/-}$.Cav1$^{-/-}$ mice exhibited a blunted hepatic gluconeogenesis, leading to the accumulation of hepatic G6P, glycogen and TG levels without a compensatory increase in intrahepatic glucose levels. The same characteristic phenotype was observed in mice with a total suppression of HGP (L.G6pc$^{-/-}$ mice, carrying a liver-specific deletion of *G6pc1*) [46]. L.G6pc$^{-/-}$ mice exhibited increased hepatic G6P concentration, which promoted the remodeling of cellular metabolism [48] (e.g. low intracellular glucose levels, increased hepatic glycogen and triglyceride (TG) levels in 16 h-fasted mice (Supplemental Fig. 4B and [31]). Of note, L.G6pc$^{-/-}$ hepatocytes had a residual glucose production through glycogen debranching [32], which might also take place in L. Glut2$^{-/-}$.Cav1$^{-/-}$ mice (Supplemental Fig. 4C).

L.G6pc$^{-/-}$ mice maintain their glycaemia thanks to the induction of kidney and intestine gluconeogenesis [46]. We thus studied whether extra-hepatic production of glucose were increased in L. Glut2$^{-/-}$.Cav1$^{-/-}$ mice. To this end, we performed a glutamine tolerance test, since glutamine is predominantly a renal and intestinal gluconeogenic substrate and is minorly used by the liver for gluconeogenesis [36,49]. Blood glucose levels were increased during the glutamine tolerance test in L. Glut2$^{-/-}$.Cav1$^{-/-}$ mice as compared to WT, Cav1$^{-/-}$ or L. Glut2$^{-/-}$ mice, suggesting an increased participation of the kidney and intestine in glucose production in the double knockout mice (Fig. 1G). Consistently, after 16 h of fasting, L. Glut2$^{-/-}$.Cav1$^{-/-}$ mice maintained their glycaemia at the same level as WT and L. Glut2$^{-/-}$ mice (Fig. 1H), despite a much weaker production of glucose from hepatocytes (Fig. 1A).

To sum up, L. Glut2$^{-/-}$.Cav1$^{-/-}$ mice recapitulated the phenotype characteristic of L.G6pc$^{-/-}$ mice, [46]. This demonstrates that gluconeogenesis (at the step catalyzed by G6Pase or immediately downstream) was decreased in the absence of Cav1 and virtually suppressed in the absence of both hepatic GLUT2 and Cav1 proteins. We then further explored how Cav1 might control the capacity of G6Pase to produce glucose.

3.3. Caveolin-1 colocalizes but does not interact with G6PC1

Outside caveolae, Cav1 can regulate the activity and signaling capacity of several transmembrane proteins through a direct interaction [24,47]. We thus hypothesized that Cav1 may directly interact with G6Pase, and more particularly with its catalytic subunit G6PC1. Using immunofluorescence experiments, we first showed that about 20% of endogenous G6PC1 (red) colocalized with endogenous Cav1 (green) in primary hepatocytes isolated from WT livers (Figure 2A,B). We then focused on the possible physical interaction between Cav1 and G6PC1. The analysis of the G6PC1 amino acid sequence predicted the existence of one consensus Cav1-binding motif (CBM), $\Phi X\Phi XXXX\Phi$/$\Phi XXXX\Phi XX\Phi$, where Φ is an aromatic amino acid W, F, or Y [24], well-conserved in mammals (Supplemental Table S1) and facing cytoplasm (Supplemental Fig. 5A). We studied the physical interaction of G6PC1 with Cav1 by immunoprecipitating endogenous Cav1 from WT and Cav1$^{-/-}$ liver (Fig. 2C). As expected, we detected Cav1 in the precipitate from WT liver but not in the precipitate from Cav1$^{-/-}$ liver (Figure 2C, right panel). However, G6PC1 was neither detected in the precipitate from WT nor Cav1$^{-/-}$ liver (Figure 2C, left panel). Taken together, these results demonstrate that G6PC1 partially colocalizes but might not physically interact with Cav1 in mouse liver.

3.4. The intracellular G6PC1 localization in the secretory pathway is controlled by Caveolin-1

In addition to a control by direct interaction, Cav1 regulates the activity of several transmembrane proteins by controlling their localization in the ER and Golgi complex [50,51] and their trafficking along the secretory pathway to the plasma membrane (PM) [23]. We thus studied whether Cav1 might control the intracellular localization of G6PC1 in the different compartments of the secretory pathway: ER, Golgi complex and PM. Immunostaining analyses of liver sections of WT and Cav1$^{-/-}$ mice showed that G6PC1 (in red) colocalized with the ER marker Calnexin (in green, Fig. 2D). Quantification of this colocalization, using the Pearson correlation coefficient, showed that the absence of Cav1 had no effect on the localization of G6PC1 in the ER (Fig. 2E). A small fraction of G6PC1 (in red) was also colocalized with the Golgi complex marker Giantin (in yellow, Fig. 2F) and the plasma membrane marker wheat germ agglutinin (WGA) (in green, Fig 2H). Interestingly, quantification showed a reduction of G6PC1 localization in the Golgi complex of Cav1$^{-/-}$ liver compared to WT liver (Fig. 2G). Of note, the amount of Giantin did not differ between WT and Cav1$^{-/-}$ liver sections (WT $= 4352 \pm 312$ vs Cav1$^{-/-}$ $= 4515 \pm 257$ pixel value/μm^2). The colocalization of G6PC1 with WGA was too low to use the Pearson correlation coefficient for quantification. We thus extracted PM fractions from differential centrifugations of WT and Cav1$^{-/-}$ liver homogenates. Western-blot analyses of the PM fractions confirmed the localization of G6PC1 at the PM, which was decreased by about 50% in PM fractions of Cav1$^{-/-}$ compared to WT liver (Figure 2I,J). Plasma membrane fractions from WT liver contained Cav1 (Fig. 2K). The presence of endogenous G6PC1 at the membrane of hepatocyte villi was also confirmed by gold immunostaining coupled to TEM. Using this technique, we also evidenced a decrease of G6PC1 at the hepatocyte villi of Cav1$^{-/-}$ compared to WT mice (Supplemental Figs. 5B–D). Of note, G6PT was also detected in PM fractions of mouse liver but its proportion here was not different in the absence of Cav1 (Fig. 2L, G6PT in % of WT: WT 100 ± 22.8 vs Cav1$^{-/-}$ 128.4 ± 40.7). These data indicate that the amount of G6PC1 at the PM depended on Cav1 and suggest that Cav1 controlled G6PC1 transport to the plasma membrane. It is noteworthy that the localization of the basolateral

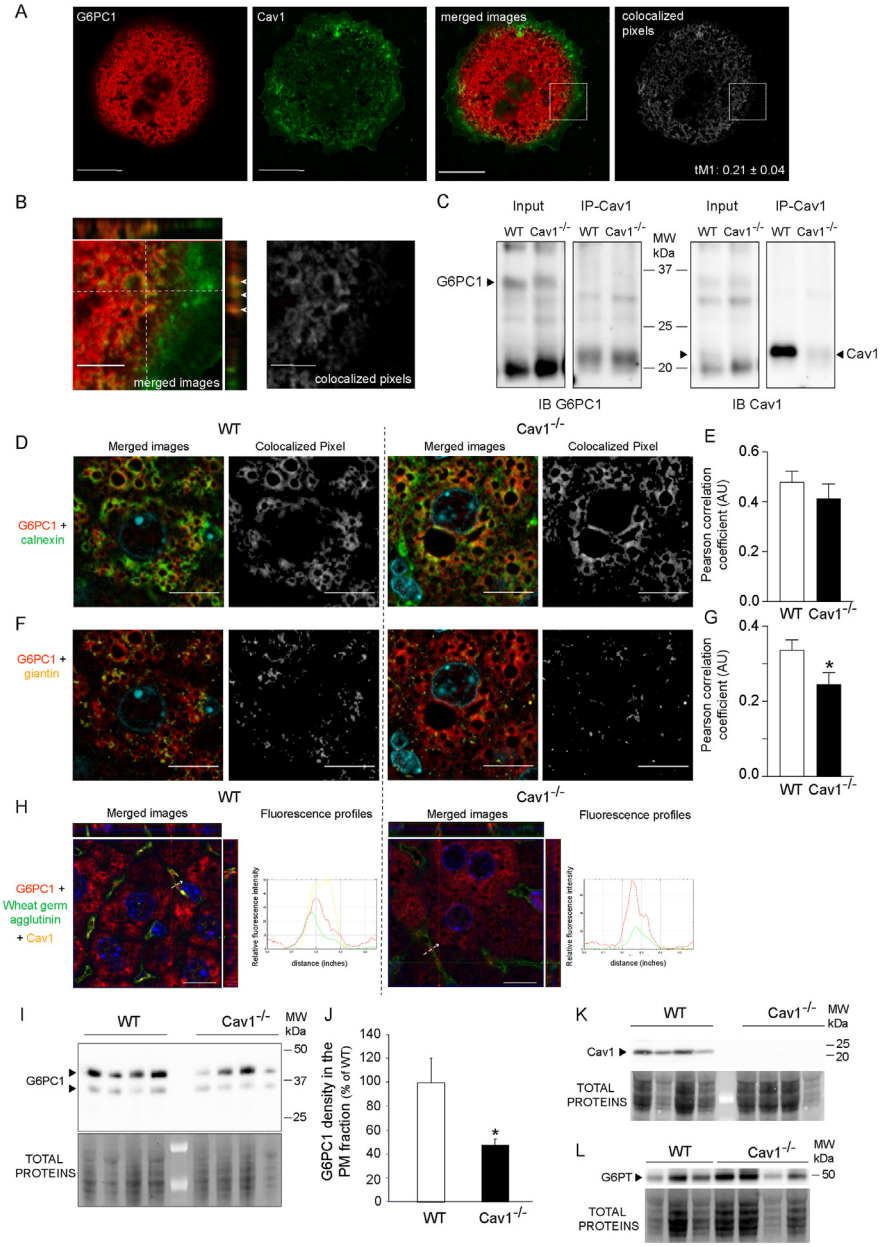

Figure 2: ***Caveolin-1 colocalizes but does not interact with G6PC1.*** (A) Representative confocal microscopy images of endogenous G6PC1 (red) and Cav1 (green) in a primary hepatocyte. Scale bar = 20 μm. Colocalized pixel from merged images are indicated in grey in the right panel. Manders coefficient (M1) indicates the fraction of G6PC1 signal colocalized with Cav1 signal. Data are mean ± s. e.m, n = 7. (B) Higher magnification of the cell part delimited by a dotted line square. Inset on top shows the orthogonal view along the z-axis on the vertical line and inset on the right shows the orthogonal view along the z-axis of the horizontal line. White arrowheads indicate colocalized G6PC1 and Cav1 signals. Colocalized pixel from merged images (left) are indicated in grey in the right panel. Scale bar = 5 μm. (C) Representative immunoprecipitation experiments performed from WT and Cav1$^{-/-}$ mouse liver. Molecular weights are indicated on the middle of the pictures. Immunoprecipitation of Cav1 was followed by immunoblotting against G6PC1 (left panel) or against Cav1 (right panel). Arrowheads indicate specific bands. Input lanes represent about 2% of the protein lysates used for IP. See also Supplemental Figs. 2 and 5. (D, F) Representative confocal images of endogenous G6PC1 (red) and (D) calnexin (green) or (F) giantin (yellow) in WT and Cav1$^{-/-}$ liver. Nuclei are stained in blue. Scale bar = 10 μm (D, F) Quantification of the colocalization of G6PC1 with calnexin (E) or giantin (G) using the Pearson correlation coefficient. Data are means ± s. e.m of n = 6 mouse livers. *p < 0.05: significant differences between WT and Cav1$^{-/-}$ mice, unpaired Student's t-test. (H) Representative confocal images of endogenous G6PC1 (red), Cav1 (yellow) and wheat germ agglutinin (WGA) (green) in WT and Cav1$^{-/-}$ liver section. Nuclei are stained in blue. Colocalizations can be seen in merged images and on the graph showing the relative fluorescence profiles of G6PC1, Cav1 and WGA (fluorescence intensities were plotted against the distance along the white dotted lines shown on the merged channel image). Inset on top of the merged channel image shows the orthogonal view along the z-axis on the vertical line and inset on the right shows the orthogonal view along the z-axis of the horizontal line. Scale bar = 10 μm. (I) Western-blot images of G6PC1 in plasma membrane fractions from WT and Cav1$^{-/-}$ liver and of the total proteins used for normalization. Molecular weights are indicated on the right of the images. (J) Relative amount of G6PC1 in plasma membrane fractions from WT (white bar) and Cav1$^{-/-}$ (black bar) liver. Data are expressed as % of WT values and are mean ± s. e.m of n = 4 mice per group. *p < 0.01: significant differences between WT and Cav1$^{-/-}$, unpaired Student's *t* test. Western-blot images of Cav1 (K) and G6PT (L) in plasma membrane fractions from WT and Cav1$^{-/-}$ liver and of the total proteins used for normalization. Molecular weights are indicated on the right of the images.

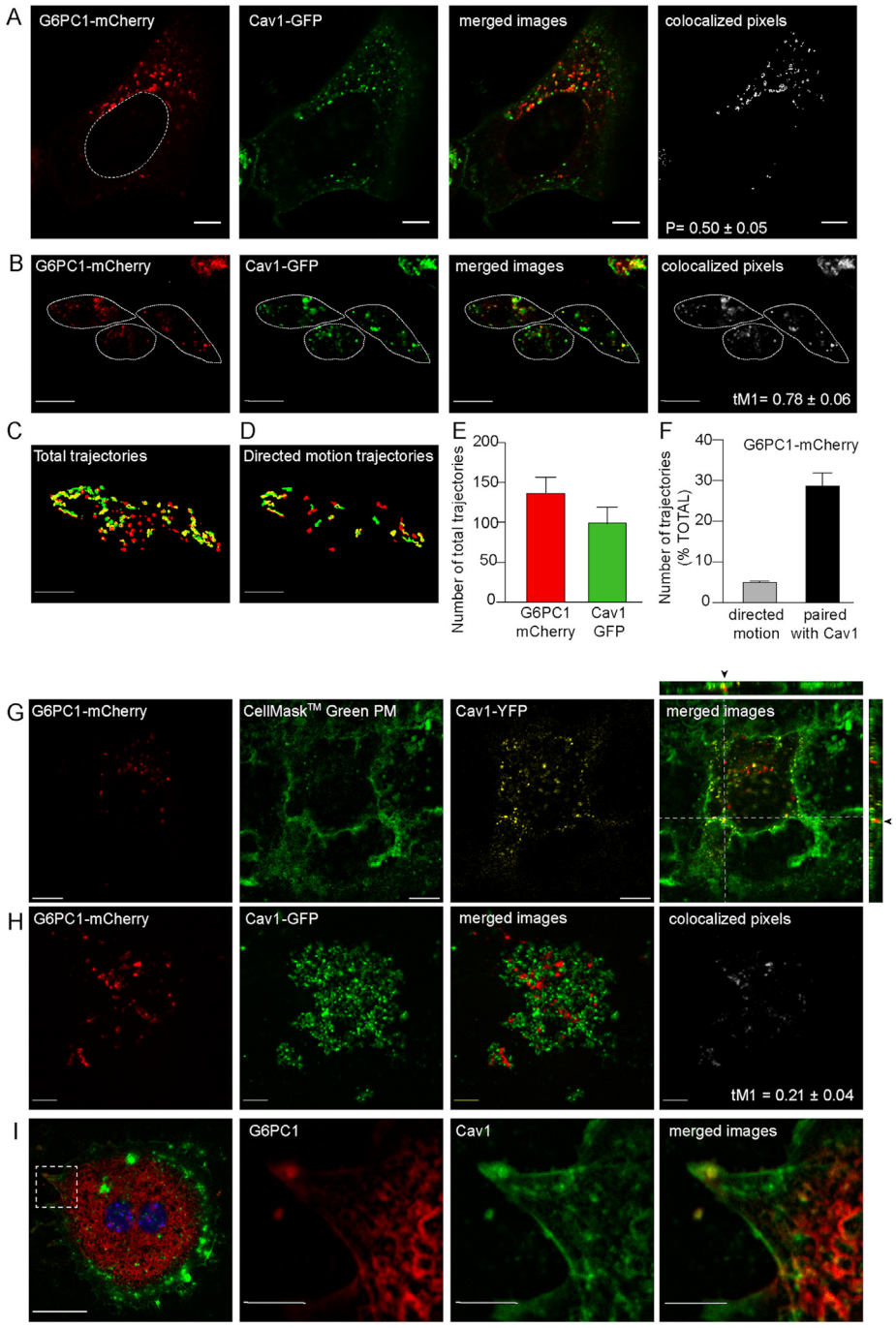

Figure 3: ***Caveolin-1 and G6PC1 move in cells and colocalize at the plasma membrane.*** (A—B) Representative images of living HepG2 cells expressing G6PC1-mCherry (red) and Cav1-GFP (green). Dotted lines are indicator of nucleus (A) or cell membranes (B). Colocalizations can be seen in merged images or in the panel showing the colocalized pixels. Colocalized pixels are quantified using the Pearson correlation coefficient (A) or the Manders coefficient (M1) (B). Data are mean ± s. e.m of n = 7 real-time acquisitions. See also Supplemental Fig. 6. (C—D) Trajectories of G6PC1 (red) and Cav1 (green) in total (C) or exhibiting directed motion (D) from a representative real-time acquisition. Scale bar = 20 μm. (E) Number of total G6PC1 (red bar) and Cav1 (green bar) trajectories. (F) Number of G6PC1 trajectories exhibiting directed motion (grey bar) or paired with Cav1 trajectories (black bar) expressed as % of total G6PC1 trajectories. Data are means ± s. e.m of n = 7 acquisitions. See also Supplemental Video 1. (G) Representative confocal microscopy images of G6PC1-mCherry (red), Cav1-YFP (yellow) and the CellMaskTM Green Plasma membrane marker (green) in HepG2 cells. Colocalizations can be seen in merged images. Inset on top shows the orthogonal view along the z-axis on the vertical line and inset on the right shows the orthogonal view along the z-axis of the horizontal line. Black arrowheads indicate colocalized G6PC1 and Cav1 at the plasma membrane. Scale bar = 10 μm. (H) Representative TIRF microscope images of G6PC1-mCherry (red) and Cav1-GFP (green) at the plasma membrane of HepG2 cells. Colocalizations can be seen in merged images or in the panel showing the colocalized pixels. Manders coefficient (M1) indicates the fraction of G6PC1 signal colocalized with Cav1 signal. Data are mean ± s. e.m, n = 3. Scale bar = 10 μm. See also Supplemental Video 2. (I) Representative confocal microscopy image of primary hepatocyte immunolabelling, scale bar = 20 μm. Higher magnification images of the part delimited by a dotted line square highlight endogenous G6PC1 (red) and Cav1 (green) localized at the plasma membrane. Colocalizations can be seen in the merged image. Scale bar = 5 μm.

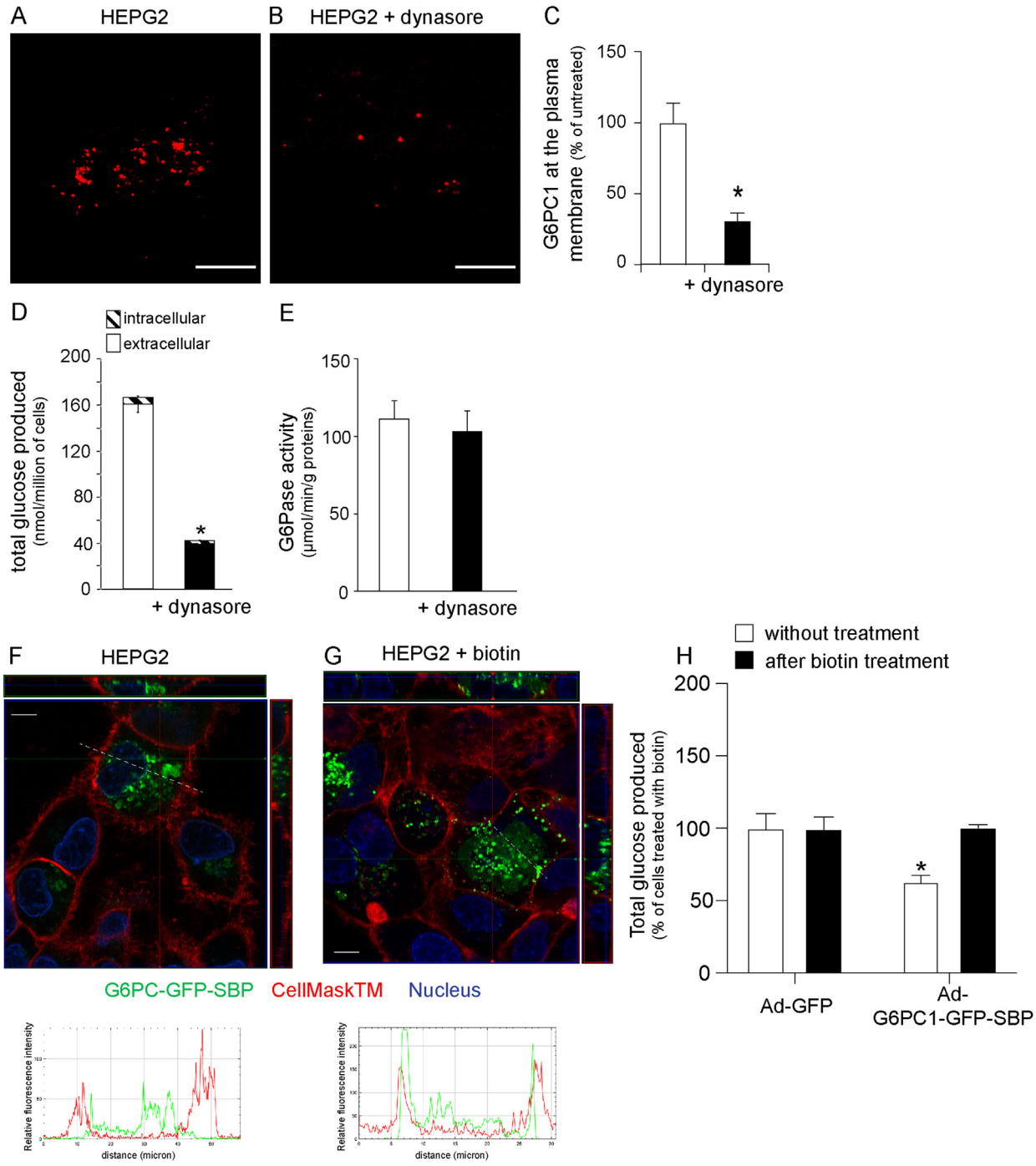

Figure 4: ***Avoiding G6PC1 to reach the plasma membrane reduces gluconeogenesis.*** (A—B) Representative TIRF microscopy images of G6PC1-mCherry overexpressed in HepG2 cells (A) or 30 min after 80 µM dynasore treatment (B). Scale bar = 10 µm. (C) Quantification of the amount of G6PC1 labelling located at the plasma membrane (white bar) or 30 min after 80 µM dynasore treatment (black bar). Data are means ± s. e.m. from 8 cells per condition and are expressed as % of the values obtained in untreated cells. (D) Total glucose produced from 1 mM pyruvate and 10 mM lactate by WT hepatocytes treated (white bar) or not (black bar) with 80 µM dynasore. Open bars represent extracellular glucose while hatched bars represent intracellular glucose. See also Supplemental Fig. 7. (E) G6Pase activity of WT hepatocytes treated (white bar) or not (black bar) with 80 µM dynasore. Data are means ± s. e.m. from 7 mice per group. Significant differences between untreated and treated cells are indicated as * $p < 0.01$, unpaired Student's t-test. (F—G) Representative confocal microscope images of the G6PC-GFP-SBP construct (green) overexpressed in HepG2 cells before (F) or after (G) 2 h of treatment with 80 µM biotin in the culture medium. Nuclei are stained in blue and cell membrane in red with CellMaskTM Red Plasma membrane marker. Scale bar = 10 µm. Inset on top of the merged channel image shows the orthogonal view along the z-axis on the vertical line and inset on the right shows the orthogonal view along the z-axis of the horizontal line. Fluorescence intensities of G6PC1 (green) and CellMaskTM Red Plasma membrane marker (red) were plotted against the distance along the white dotted lines shown on the merged channel image. (H) Total glucose produced from 1 mM pyruvate before (white bars) or after (black bars) biotin treatment in HepG2 cells overexpressing Ad-GFP or Ad-G6PC-GFP-SBP constructs. Data are expressed as % of the glucose produced after biotin treatment and are means ± s. e.m. from 6 experiments. Significant differences between before and after treatment are indicated as * $p < 0.01$, two-way ANOVA followed by Tukey's post hoc test. See also Supplemental Fig. 8.

protein Na/K ATPase and the amount of the plasma membrane protein E-Cadherin were not changed by the Cav1 deficiency (Supplemental Figs. 5E and F), indicating that the alteration of the G6PC1 localization at the plasma membrane of the Cav1$^{-/-}$ liver was not due to a general mislocalization of transmembrane proteins. Finally, we used chimeric constructs of G6PC1 and Cav1 to study protein trajectories in living cells. When overexpressed in the hepatoma cells HepG2, G6PC1 coupled to mCherry (G6PC1-mCherry) had the same localization pattern as endogenous G6PC1 and colocalized with ER markers (Supplemental Figs. 6A and B) and with Cav1 coupled to green fluorescent protein (Cav1-GFP) (Figure 3A) as in the liver. Live cell imaging showed that G6PC1-mCherry and Cav1-GFP moved within cells (Figure 3B,C and Supplemental Video 1). Based on their net travelled distance, we discriminated proteins exhibiting a directed motion (i.e. following a trajectory) from proteins moving around the same position over time. Only 3.5% of the G6PC1-mCherry trajectories exhibited directed motion (Figure 3D, green trajectories and Figure 3F, grey bar). More interestingly, about 30% of the total G6PC1-mCherry trajectories were associated with Cav1-GFP trajectories (Figure 3F, black bar). The directional movement of some of these trajectories suggested that both proteins colocalized at the plasma membrane. Colocalization of G6PC1-mCherry and Cav1-YFP with a plasma membrane marker indeed demonstrated that few G6PC1 signals were localized at the plasma membrane together with Cav1 (Fig. 3G). To better define this localization, we used total internal reflection fluorescence (TIRF) microscopy, so as to restrict cell imaging to the vicinity of the plasma membrane. Total internal reflection fluorescence microscopy imaging illustrated that G6PC1-mCherry appeared transiently at the plasma membrane (Figure 3H and Supplemental Video 2). Using the Manders coefficient, we calculated that 21% of G6PC1-mCherry proteins colocalized with Cav1-GFP at the plasma membrane (Fig. 3H). Importantly, G6PC1 was also found colocalized with Cav1 at the plasma membrane of mouse hepatocytes (Figure 3I,E).

3.5. Preventing G6PC1 from reaching the plasma membrane reduces gluconeogenesis

Finally, we asked whether the capacity of G6PC1 to be transported at the plasma membrane was associated with glucose production by hepatocytes. To this end, we used dynasore, previously known as an inhibitor of dynamins, but nowadays considered as a broad inhibitor of vesicular pathways between the ER and PM [52] or between endosomes and the ER [53]. Noteworthy, the amount of G6PC1-mCherry present at the PM, quantified by TIRF microscopy, was decreased by 70% in the presence of dynasore (Figure 4A—C). In parallel, we tested whether the decrease in G6PC1 amount at the PM induced by dynasore was capable of altering glucose production by hepatocytes. Dynasore treatment decreased glucose production from primary hepatocytes (Fig. 4D), without affecting total G6Pase activity assayed at Vmax (Fig. 4E), as previously observed in Cav1$^{-/-}$ hepatocytes (Supplemental Fig. 4A). Importantly, this decrease in glucose production depended on the inhibition of vesicle trafficking, since dynasore treatment did not further decrease glucose production in hepatocytes treated at 21 °C (Supplemental Fig. 7A). This decrease was also independent of GLUT2, since dynasore treatment still decreased glucose production from primary hepatocytes lacking the GLUT2 transporter (Supplemental Fig. 7B). To specifically inhibit G6PC1 release from the ER, we then used the retention using selective hooks (RUSH) system [33]. RUSH is based on the reversible interaction of a hook protein fused to core streptavidin and stably anchored in a chosen compartment with a protein of interest fused to streptavidin-binding peptide (SBP). Biotin addition causes a synchronous release of the protein of interest from the hook. In our experiment, we used the human invariant chain of the major histocompatibility complex (Ii; a type II protein) stably present in the ER as a hook. This transmembrane protein was fused to core streptavidin in its cytoplasmic region (Str_Ii). In parallel, the cytoplasmic C-terminal part of G6PC1 was fused to SBP and GFP (G6PC1-SBP-GFP) (Supplemental Fig. 8A). Chimeric proteins were expressed from a single plasmid designed to induce a stochiometric overexpression of both constructs [33]. When overexpressed in HepG2 cells in the absence of biotin, G6PC1-SBP-GFP proteins were retained in the ER (Supplemental Fig. 8 B,C) and conserved G6Pase activity (G6PC1-SBP-GFP 29.4 $\pm$ 2.9 vs VSVG-SBP-GFP 0.00 $\pm$ 0.07 nmol/min/mg proteins). In the absence of biotin, the G6PC1-SBP-GFP construct did not localize at the plasma membrane of HepG2 cells (Fig. 4F). After the addition of biotin, G6PC1-SBP-GFP proteins were released from the ER and found localized at the PM of HepG2 cells (Fig. 4G). More importantly, the retention of G6PC1 in the ER produced a 37% decrease in glucose production (Fig. 4H). Taken together, our results demonstrate that the capacity of G6PC1 to reach the PM controlled glucose production from hepatocytes.

4. DISCUSSION

Despite the relative low amount of caveolae in hepatocytes [54], Cav1 has recently emerged as an important regulator of liver function [24], through the modulation of several molecular pathways including lipid storage [27], mitochondrial biology [27], and liver regeneration [55]. In particular, Cav1 has been suggested to play a crucial role in maintaining hepatic lipid metabolism during adaptation to fasting [27]. Here, we decipher a pathway implicated in HGP, depending on the capacity of G6PC1 to be transported to the PM by a mechanism controlled by Cav1. We clearly demonstrate that the absence of Cav1 leads to a decrease in glucose production, resulting in a small accumulation of G6P in hepatocytes. In agreement with our data, the specific suppression of Cav1 in the liver leads to a decrease in plasma glucose levels in the fasting state [27,56]. Moreover, we decipher the molecular regulation of a vesicular pathway controlling HGP, the existence of which was first suggested in Glut2$^{-/-}$ mice 25 years ago but still uncharacterized [21]. Using L. Glut2$^{-/-}$ crossbred with Cav1$^{-/-}$ mice, we assess the relative roles of the Cav1-dependent and GLUT2-dependent glucose production pathways. Interestingly, L. Glut2$^{-/-}$.Cav1$^{-/-}$ mice develop the same phenotype as mice lacking hepatic G6PC1 (L.G6pc$^{-/-}$ mice). The Cav1-and GLUT2-dependent pathways can thus be considered as two major independent pathways enabling the release of “gluconeogenic” glucose from the liver. Interestingly, Cav1$^{-/-}$ hepatocytes produced less glucose without a proportional accumulation of intracellular glucose, suggesting that the lack of Cav1 results in a decrease in glucose production at the level of G6Pase. The discrepancy between the G6Pase activity assayed *in vitro* at Vmax and the effective G6Pase activity occurring *in situ*, estimated from glucose production, has already been suggested: several hypotheses involving lipid composition of the membrane [13] or membrane fluidity were proposed to account for G6Pase substrate specificity within the first seconds of the enzymatic reaction [57] and for the stimulation of G6Pase activity by glucagon [19,20]. However, no molecular mechanism accounting for these regulations has been proposed yet. In this context, we demonstrate that the G6Pase capacity to produce glucose depends on the trafficking of G6PC1 to the PM

through a Cav1-dependent mechanism. We show that this mechanism is specific to G6PC1 since the localization of other plasma membrane proteins (Na/K ATPase and E-Cadherin) or of the other protein involved in the G6Pase function (G6PT) was not changed in the absence of Cav1. It is noteworthy that previous biochemical studies suggested that an unidentified 21 kDa protein (which corresponds to the molecular weight of Cav1) associated with ER membranes controls G6Pase activity [58]. However, we failed to demonstrate that endogenous G6PC1 physically interacts with Cav1. This could be due to the difficulty to detect the low proportion of G6PC1 interacting with Cav1 (around 20%) in the liver. Biochemical studies hypothetically linked the structural particularities of the membrane surrounding the G6Pase complex to its capacity to produce glucose [59,60]. We might thus suggest that Cav1 promotes changes in lipid species in the vicinity of G6PC1, which could facilitate its incorporation in the pathway of moving to the PM.

More importantly, we demonstrated that G6PC1 and Cav1 colocalized at the PM of hepatocytes. We detected G6PC1 at the villi of the basolateral membrane of hepatocytes, where the glucose transporter GLUT2 exports glucose from the cell to the blood [61], and where Cav1 is localized [54]. We also detected G6PT at the PM. This location should ensure the coupling of G6P transport to G6P hydrolysis (which is a hallmark of G6Pase [62]), by delivering G6P to the G6PC1 catalytic site profoundly buried in the membrane. In agreement with these data, a small amount of G6Pase activity was previously suggested to be associated with PM fractions of rat liver. The amount of G6PC1 present at this site could directly control a substantial fraction of glucose production. Consistently, we showed that cells produced more glucose when G6PC1 was allowed to reach the plasma membrane than when it was retained in the ER. We thus hypothesize that G6PC1 might couple glucose production and subsequent release at the plasma membrane. In conclusion, we provide here new evidence that hepatic G6Pase activity is tightly controlled by its intracellular localization, *via* a process depending on Cav1. We show that the transport of G6PC1 from the ER to the PM is required for the full production of glucose in the fasting state. It is noteworthy that these data document the previous questioning about the physiological sense of the presence of G6PC1 within the ER membrane. Therefore, the mechanism described here provides new knowledge in relation with HGP, which might be of prime importance in situations of increased or under-repressed glucose production, such as metabolic diseases and type 2 diabetes.

FUNDING

This work was supported by a research grant from the French National Research Agency (Projet-ANR-17-CE14-0026).

AUTHOR CONTRIBUTION

AGS conducted the conceptualization, methodological choices and experiments, supervised the study and wrote the manuscript. JC contributed to the conceptualization, methodological choices and experiments, and reviewed the manuscript. MS and CL contributed to the conceptualization of the study and edited the manuscript. BT provided $Glut2^{lox/lox}$ mice and reviewed the manuscript. CP contributed to the TIRFM experiments. CZ, AD and LDC contributed to the experiments. FR reviewed and edited the manuscript. GM contributed to the conceptualization, the interpretation of data and the writing of the manuscript. AGS and GM are the guarantors of this work and, as such, had full access to all the data in the study and take responsibility for the integrity of the data and the accuracy of the data analysis.

DECLARATION OF COMPETING INTEREST

The authors declare the following financial interests/personal relationships which may be considered as potential competing interests: Amandine Gautier-Stein reports financial support was provided by French National Research Agency.

DATA AVAILABILITY

Data will be made available on request.

ACKNOWLEDGMENTS

The authors used the SFR Lyon Est facilities (CNRS UMS3453 - INSERM US7, Lyon) and particularly thank the members of the "Animalerie Lyon Est Conventionnelle et SPF" for animal care and the members of the CIQLE platforms for TEM (Elisabeth Errazuriz-Cerda) and confocal imaging. The authors used the PLATIM SFR Biosciences facility (UMS3444/CNRS, US8/Inserm, ENS de Lyon, UCBL) and acknowledge Christophe Chamot for live imaging. The authors thank Ari Helenius for providing the Cav1-GFP plasmid, Antoine Font for his help in imaging studies, Nicolas Chenouard for his insightful advices for trajectory analyses and Mélanie Paillard and Ludovic Gomez for their help in PM extractions. The authors thank the INRAE (AGS), CNRS (GM, FR) and Inserm (CZ, AD) for funding their positions. Finally, they thank the Ministère de l'Enseignement Supérieur et de la Recherche for funding JC's position as a PhD student.

APPENDIX A. SUPPLEMENTARY DATA

Supplementary data to this article can be found online at https://doi.org/10.1016/j.molmet.2023.101700.

REFERENCES

[1] Rizza RA. Pathogenesis of fasting and postprandial hyperglycemia in type 2 diabetes: implications for therapy. Diabetes 2010;59(11):2697—707. Nov.
[2] Soty M, Gautier-Stein A, Rajas F, Mithieux G. Gut-brain glucose signaling in energy homeostasis. Cell Metabol 2017;25(6):1231—42. Jun 6.
[3] Abdul-Wahed A, Gautier-Stein A, Casteras S, Soty M, Roussel D, Romestaing C, et al. A link between hepatic glucose production and peripheral energy metabolism via hepatokines. Mol Metabol 2014;3(5):531—43.
[4] Clore JN, Stillman J, Sugerman H. Glucose-6-phosphatase flux in vitro is increased in type 2 diabetes. Diabetes 2000;49(6):969—74.
[5] van Schaftingen E, Gerin I. The glucose-6-phosphatase system. Biochem J 2002;362(Pt 3):513—32.
[6] Thorens B, Mueckler M. Glucose transporters in the 21st century. Am J Physiol Endocrinol Metab 2010;298(2):E141—5. Feb.
[7] Hers HG, Berthet J, Berthet L, De Duve C. [The hexose-phosphatase system. III. Intracellular localization of enzymes by fractional centrifugation]. Bull Soc Chim Biol (Paris) 1951;33(1—2):21—41.
[8] Nordlie RC, Arion WJ. Evidence for the common identity of glucose 6-PHOSPHATASE, inorganic pyrophosphatase, and pyrophosphate-glucose phosphotransferase. J Biol Chem 1964;239:1680—5. Jun.
[9] Garfield SA, Cardell RR. Hepatic glucose-6-phosphatase activities and correlated ultrastructural alterations in hepatocytes of diabetic rats. Diabetes 1979;28(7):664—79. Jul.
[10] Lei KJ, Pan CJ, Shelly LL, Liu JL, Chou JY. Identification of mutations in the gene for glucose-6-phosphatase, the enzyme deficient in glycogen storage disease type 1a. J Clin Invest 1994;93(5):1994—9. May.
[11] Chen LY, Lin B, Pan CJ, Hiraiwa H, Chou JY. Structural requirements for the stability and microsomal transport activity of the human glucose 6-phosphate transporter. J Biol Chem 2000;275(44):34280—6. Nov.

[12] Soty M, Chilloux J, Casteras S, Grichine A, Mithieux G, Gautier-Stein A. New insights into the organisation and intracellular localisation of the two subunits of glucose-6-phosphatase. Biochimie 2012;94(3):695–703.
[13] Mithieux G. New knowledge regarding glucose-6 phosphatase gene and protein and their roles in the regulation of glucose metabolism. Eur J Endocrinol 1997;136(2):137–45.
[14] Bady I, Zitoun C, Guignot L, Mithieux G. Activation of liver G-6-Pase in response to insulin-induced hypoglycemia or epinephrine infusion in the rat. Am J Physiol Endocrinol Metab 2002;282(4):E905–10.
[15] Daniele N, Bordet JC, Mithieux G. Unsaturated fatty acids associated with glycogen may inhibit glucose-6 phosphatase in rat liver. J Nutr 1997;127(12):2289–92.
[16] Daniele N, Rajas F, Payrastre B, Mauco G, Zitoun C, Mithieux G. Phosphatidylinositol 3-kinase translocates onto liver endoplasmic reticulum and may account for the inhibition of glucose-6-phosphatase during refeeding. J Biol Chem 1999;274(6):3597–601.
[17] Guignot L, Mithieux G. Mechanisms by which insulin, associated or not with glucose, may inhibit hepatic glucose production in the rat. Am J Physiol 1999;277(6 Pt 1):E984–9.
[18] Mithieux G, Daniele N, Payrastre B, Zitoun C. Liver microsomal glucose-6-phosphatase is competitively inhibited by the lipid products of phosphatidylinositol 3-kinase. J Biol Chem 1998;273(1):17–9.
[19] Ichai C, Guignot L, El-Mir MY, Nogueira V, Guigas B, Chauvin C, et al. Glucose 6-phosphate hydrolysis is activated by glucagon in a low temperature-sensitive manner. J Biol Chem 2001;276(30):28126–33.
[20] Soty M, Chilloux J, Delalande F, Zitoun C, Bertile F, Mithieux G, et al. Post-translational regulation of the glucose-6-phosphatase complex by cyclic adenosine monophosphate is a crucial determinant of endogenous glucose production and is controlled by the glucose-6-phosphate transporter. J Proteome Res 2016;15(4):1342–9. Apr 1.
[21] Guillam MT, Burcelin R, Thorens B. Normal hepatic glucose production in the absence of GLUT2 reveals an alternative pathway for glucose release from hepatocytes. Proc Natl Acad Sci U A 1998;95(21):12317–21.
[22] Hosokawa M, Thorens B. Glucose release from GLUT2-null hepatocytes: characterization of a major and a minor pathway. Am J Physiol Endocrinol Metab 2002;282(4):E794–801.
[23] Lamaze C, Tardif N, Dewulf M, Vassilopoulos S, Blouin CM. The caveolae dress code: structure and signaling. Curr Opin Cell Biol 2017;47:117–25. Aug.
[24] Pol A, Morales-Paytuví F, Bosch M, Parton RG. Non-caveolar caveolins – duties outside the caves. J Cell Sci 2020;133(9):jcs241562. May 1.
[25] Porta JC, Han B, Gulsevin A, Chung JM, Peskova Y, Connolly S, et al. Molecular architecture of the human caveolin-1 complex. Sci Adv 2022;8(19):eabn7232. May 13.
[26] Parton RG, McMahon KA, Wu Y. Caveolae: formation, dynamics, and function. Curr Opin Cell Biol 2020;65:8–16. Aug.
[27] Asterholm IW, Mundy DI, Weng J, Anderson RGW, Scherer PE. Altered mitochondrial function and metabolic inflexibility associated with loss of caveolin-1. Cell Metabol 2012;15(2):171–85. Feb 8.
[28] Fernández-Rojo MA, Gongora M, Fitzsimmons RL, Martel N, Martin SD, Nixon SJ, et al. Caveolin-1 is necessary for hepatic oxidative lipid metabolism: evidence for crosstalk between caveolin-1 and bile acid signaling. Cell Rep 2013;4(2):238–47. Jul 25.
[29] Pol A, Martin S, Fernandez MA, Ferguson C, Carozzi A, Luetterforst R, et al. Dynamic and regulated association of caveolin with lipid bodies: modulation of lipid body motility and function by a dominant negative mutant. Mol Biol Cell 2004;15(1):99–110. Jan.
[30] Seyer P, Vallois D, Poitry-Yamate C, Schütz F, Metref S, Tarussio D, et al. Hepatic glucose sensing is required to preserve β cell glucose competence. J Clin Invest 2013;123(4):1662–76. Apr.
[31] Mutel E, Abdul-Wahed A, Ramamonjisoa N, Stefanutti A, Houberdon I, Cavassila S, et al. Targeted deletion of liver glucose-6 phosphatase mimics glycogen storage disease type 1a including development of multiple adenomas. J Hepatol 2011;54(3):529–37. Mar.
[32] Hijmans BS, Boss A, van Dijk TH, Soty M, Wolters H, Mutel E, et al. Hepatocytes contribute to residual glucose production in a mouse model for glycogen storage disease type Ia: hijmans et al. Hepatology 2017;66(6):2042–54. Dec.
[33] Boncompain G, Divoux S, Gareil N, de Forges H, Lescure A, Latreche L, et al. Synchronization of secretory protein traffic in populations of cells. Nat Methods 2012;9(5):493–8. Mar 11.
[34] Tagawa A, Mezzacasa A, Hayer A, Longatti A, Pelkmans L, Helenius A. Assembly and trafficking of caveolar domains in the cell: caveolae as stable, cargo-triggered, vesicular transporters. J Cell Biol 2005;170(5):769–79.
[35] Bergmeyer HU, Bernt E, Schmidt F, Stork M. D-glucose. In: Bergmeyer HU, editor. Methods of Enzymatic Analysis. vol. 3. Academic Press New York; 1974. p. 1196–201.
[36] Croset M, Rajas F, Zitoun C, Hurot JM, Montano S, Mithieux G. Rat small intestine is an insulin-sensitive gluconeogenic organ. Diabetes 2001;50(4):740–6.
[37] Minassian C, Mithieux G. Differential time course of liver and kidney glucose-6 phosphatase activity during fasting in rats. Comp Biochem Physiol B Biochem Mol Biol 1994;109(1):99–104.
[38] Lang G, Michal G. D-glucose-6-phosphate and D-fructose-6-phosphate. In: Bergmeyer HU, editor. Methods of enzymatic analysis. vol. 3. Academic Press New York; 1974. p. 1238–42.
[39] Bligh EG, Dyer WJ. A rapid method of total lipid extraction and purification. Can J Biochem Physiol 1959;37(8):911–7. Aug.
[40] Suski JM, Lebiedzinska M, Wojtala A, Duszynski J, Giorgi C, Pinton P, et al. Isolation of plasma membrane–associated membranes from rat liver. Nat Protoc 2014;9(2):312–22. Feb.
[41] Rajas F, Jourdan-Pineau H, Stefanutti A, Mrad EA, Iynedjian PB, Mithieux G. Immunocytochemical localization of glucose 6-phosphatase and cytosolic phosphoenolpyruvate carboxykinase in gluconeogenic tissues reveals unsuspected metabolic zonation. Histochem Cell Biol 2007;127(5):555–65.
[42] Sinet F, Soty M, Zemdegs J, Guiard B, Estrada J, Malleret G, et al. Dietary fibers and proteins modulate behavior via the activation of intestinal gluconeogenesis. Neuroendocrinology 2021;111(12):1249–65.
[43] Olivo-Marin JC. Extraction of spots in biological images using multiscale products. Pattern Recogn 2002;35(9):1989–96. Sep.
[44] Chenouard N, Bloch I, Olivo-Marin JC. Multiple hypothesis tracking for cluttered biological image sequences. IEEE Trans Pattern Anal Mach Intell 2013;35(11):2736–3750. Nov.
[45] Bolte S, Cordelières FP. A guided tour into subcellular colocalization analysis in light microscopy. J Microsc 2006;224(Pt 3):213–32. Dec.
[46] Mutel E, Gautier-Stein A, Abdul-Wahed A, Amigo-Correig M, Zitoun C, Stefanutti A, et al. Control of blood glucose in the absence of hepatic glucose production during prolonged fasting in mice: induction of renal and intestinal gluconeogenesis by glucagon. Diabetes 2011;60(12):3121–31.
[47] Cohen AW, Razani B, Wang XB, Combs TP, Williams TM, Scherer PE, et al. Caveolin-1-deficient mice show insulin resistance and defective insulin receptor protein expression in adipose tissue. Am J Physiol Cell Physiol 2003;285(1):C222–35. Jul.
[48] Rajas F, Gautier-Stein A, Mithieux G. Glucose-6 phosphate, A central hub for liver carbohydrate metabolism. Metabolites 2019;9(12). Nov 20.
[49] Stumvoll M, Perriello G, Meyer C, Gerich J. Role of glutamine in human carbohydrate metabolism in kidney and other tissues. Kidney Int 1999;55(3):778–92. Mar.
[50] Sasai K, Ikeda Y, Ihara H, Honke K, Taniguchi N. Caveolin-1 regulates the functional localization of N-acetylglucosaminyltransferase III within the golgi apparatus. J Biol Chem 2003;278(28):25295–301. Jul 11.
[51] Syme CA, Zhang L, Bisello A. Caveolin-1 regulates cellular trafficking and function of the glucagon-like Peptide 1 receptor. Mol Endocrinol Baltim Md 2006;20(12):3400–11. Dec.

[52] Preta G, Cronin JG, Sheldon IM. Dynasore - not just a dynamin inhibitor. Cell Commun Signal 2015;13(1):24. Dec.

[53] Girard E, Paul JL, Fournier N, Beaune P, Johannes L, Lamaze C, et al. The dynamin chemical inhibitor dynasore impairs cholesterol trafficking and sterol-sensitive genes transcription in human HeLa cells and macrophages. Hong W. PLoS One 2011;6(12):e29042. Dec 19.

[54] Calvo M, Tebar F, Lopez-Iglesias C, Enrich C. Morphologic and functional characterization of caveolae in rat liver hepatocytes. Hepatology 2001;33(5): 1259—69. May 1.

[55] Fernández MA, Albor C, Ingelmo-Torres M, Nixon SJ, Ferguson C, Kurzchalia T, et al. Caveolin-1 is essential for liver regeneration. Science 2006;313(5793):1628—32. Sep 15.

[56] Han M, Piorońska W, Wang S, Nwosu ZC, Sticht C, Wang S, et al. Hepatocyte caveolin-1 modulates metabolic gene profiles and functions in non-alcoholic fatty liver disease. Cell Death Dis 2020;11(2):104. Feb 6.

[57] Ajzannay A, Mithieux G. Glucose 6-phosphate and mannose 6-phosphate are equally and more actively hydrolyzed by glucose 6-phosphatase during hysteretic transition within intact microsomal membrane than after detergent treatment. Arch Biochem Biophys 1996;326(2):238—42. Feb 15.

[58] Burchell A, Burchell B, Monaco M, Walls HE, Arion WJ. Stabilization of glucose-6-phosphatase activity by a 21 000-dalton hepatic microsomal protein. Biochem J 1985;230(2):489—95. Sep 1.

[59] Jorgenson RA, Nordlie RC. Multifunctional glucose-6-phosphatase studied in permeable isolated hepatocytes. J Biol Chem 1980;255(12):5907—15. Jun 25.

[60] St-Denis JF, Annabi B, Khoury H, van de Werve G. Histone II-A stimulates glucose-6-phosphatase and reveals mannose-6-phosphatase activities without permeabilization of liver microsomes. Biochem J 1995;310(Pt 1): 221—4. Aug 15.

[61] Karim S, Adams DH, Lalor PF. Hepatic expression and cellular distribution of the glucose transporter family. World J Gastroenterol WJG 2012;18(46): 6771—81. Dec 14.

[62] Lei KJ, Chen H, Pan CJ, Ward JM, Mosinger Jr B, Lee EJ, et al. Glucose-6-phosphatase dependent substrate transport in the glycogen storage disease type-1a mouse. Nat Genet 1996;13(2):203—9.

